Visualizing the distributions and spatiotemporal changes of metabolites in *Panax notoginseng* by MALDI mass spectrometry imaging

Chenglong Sun [a, b, 1], Shuangshuang Ma [b, 1], Lili Li [a, b], Daijie Wang [a, b], Wei Liu [a, b], Feng Liu [a, b], Lanping Guo [c], Xiao Wang [a, b, *]

[a] School of Pharmaceutical Sciences, Qilu University of Technology (Shandong Academy of Sciences), Jinan, China
[b] Key Laboratory for Applied Technology of Sophisticated Analytical Instruments of Shandong Province, Shandong Analysis and Test Center, Qilu University of Technology (Shandong Academy of Sciences), Jinan, China
[c] Resource Center of Chinese Materia Medica, State Key Laboratory Breeding Base of Dao-di Herbs, China Academy of Chinese Medical Sciences, Beijing, China

A R T I C L E   I N F O

A B S T R A C T

Background: *Panax notoginseng* is a highly valued medicinal herb used widely in China and many Asian countries. Its root and rhizome have long been used for the treatment of cardiovascular and hematological diseases. Imaging the spatial distributions and dynamics of metabolites in heterogeneous plant tissues is significant for characterizing the metabolic networks of *Panax notoginseng*, and this will also provide a highly informative approach to understand the complex molecular changes in the processing of *Panax notoginseng*.
Methods: Here, a high-sensitive MALDI-MS imaging method was developed and adopted to visualize the spatial distributions and spatiotemporal changes of metabolites in different botanical parts of *Panax notoginseng*.
Results: A wide spectrum of metabolites including notoginsenosides, ginsenosides, amino acids, dencichine, gluconic acid, and low-molecular-weight organic acids were imaged in *Panax notoginseng* rhizome and root tissues for the first time. Moreover, the spatiotemporal alterations of metabolites during the steaming of *Panax notoginseng* root were also characterized in this study. And, a series of metabolites such as dencichine, arginine and glutamine that changed with the steaming of *Panax notoginseng* were successfully screened out and imaged.
Conclusion: These spatially-resolved metabolite data not only enhance our understanding of the *Panax notoginseng* metabolic networks, but also provide direct evidence that a serious of metabolic alterations occurred during the steaming of *Panax notoginseng*.

1. Introduction

Panax notoginseng (*P. notoginseng*) has been widely used for the treatment of cardiovascular diseases and hematological diseases in traditional Chinese medicine [1—3]. It is also regarded as an important functional food in many countries [4]. The underground parts including rhizome and root are two historically utilized medicinal portions of *P. notoginseng*. Metabolites contained in the rhizome and root of *P. notoginseng* are the material basis for *P. notoginseng* to exert its pharmacological effects. Previous studies have demonstrated that in addition to notoginsenosides and ginsenosides, the rhizome and root of *P. notoginseng* also contains dencichine, flavonoids, amino acids, organic acids, sugars, etc. [5—7].

Liquid chromatography-mass spectrometry (LC-MS) is an effective technique to investigate the metabolite profiles of biological tissues [8,9], and it has made significant inroads into the qualitative and quantitative determination of metabolites in *P. notoginseng* rhizome and root. For example, Chan et al developed

a LC-MS/MS method to confirm the structure of new saponins, and to identify artifactual and natural compounds in *Panax japonicus var. major* [1]. Jiang's group developed a high sensitive UPLC-Q-TOF mass spectrometry method to quantitatively compare eight saponins in rhizome, main root, branch root, and fibrous root of *P. notoginseng* [10]. However, it is worth noting that *P. notoginseng* possesses a high degree of heterogeneity in its tissue structure. According to the position and shape, *P. notoginseng* can be divided into rhizome, main root, branch root and fibrous root. According to the cell type and components, rhizome and root tissue can be further divided into phloem, xylem, medulla, and cork tissues. Unfortunately, the complex sample pre-treatment carried out during LC-MS analysis severely destroy the spatial information regarding the locations of metabolites in heterogeneous *P. notoginseng* tissues.

The synthesis, transport and metabolism of metabolites in higher plants are precisely regulated by their metabolic networks. The region-specific distributions of metabolites in *P. notoginseng* also lead to the different medicinal effects of different *P. notoginseng* botanical parts. In addition, both raw *P. notoginseng* and steamed *P. notoginseng* have important pharmacological effects. Traditionally, characterizing the metabolic difference between raw and steamed *P. notoginseng* requires complex tissue homogenization and metabolite extraction, and the results are often obtained by averaging the metabolite information in different parts of many *P. notoginseng* samples. This makes it difficult to accurately characterize the spatiotemporal changes of metabolites in a specific part of a certain *P. notoginseng* tissue during the steaming process. Therefore, developing a spatially-resolved method to map the distribution of metabolites in heterogeneous *P. notoginseng* tissues is very imperative, and this will essentially facilitate our understanding of the complex metabolic alteration of *P. notoginseng* during steaming.

Matrix-assisted laser desorption/ionization mass spectrometry imaging (MALDI-MSI) is a state-of-the-art tissue imaging technique, and it provides a label-free approach to localisation of different kinds of metabolites directed on the tissue sections [11–17]. Currently, MALDI-MSI technique has been successfully used to map the spatial distributions and dynamics of metabolites in different plant tissues [18–21], to visualize the complex metabolic pathways of plant secondary metabolites [22–24], and to uncover the metabolic mechanism of plants in response to biotic and abiotic stresses [25,26]. However, there are still no reports on MALDI-MSI technique to investigate the spatial distributions of metabolites in *P. notoginseng* by now. More importantly, a precise characterization of metabolites in different *P. notoginseng* botanical parts and visualizing the spatiotemporal changes of metabolites during *P. notoginseng* steaming is of great significance for elucidating the pharmacological effects of raw and steamed *P. notoginseng.*

In this study, we develop a high-sensitive MALDI-MSI method to visualize the metabolites in *P. notoginseng* tissues. The spatial distributions of notoginsenosides, ginsenosides, amino acids, dencichine, gluconic acid, and low-molecular-weight organic acids in different locations of *P. notoginseng* (including rhizome, main root, branch root and fibrous root) and in different micro-regions of *P. notoginseng* root (including phloem, xylem, medulla, and cork) were imaged for the first time. In addition, the spatiotemporal alterations of metabolites during the steaming of *P. notoginseng* root were also imaged, and a series of metabolites that changed with the steaming of *P. notoginseng* root were successfully screened out. MALDI-MS imaging of metabolites in plant tissues not only expand our understanding of the spatial features of metabolites in plants, but also provides a new approach for more detailed exploration of the molecular changes in the processing of medicinal herb.

2. Material and methods

2.1. Chemicals and reagents

1,5-Naphthalenediamine (1,5-DAN), α-cyano-4-hydroxycinnamic acid (CHCA), and 9-aminoacridine (9-AA) were obtained from Aladdin Chemical Reagent Co. (Shanghai, China). Safranin-O stain and fast green stain were provided by Beijing Solarbio Co. (Beijing, China). Tissue-Tek O.C.T. compound was purchased from Sakura Finetek Japan Co., Ltd. (Tokyo, Japan). Acetonitrile (ACN) was obtained from Merck (Muskegon, USA). Ultrapure water was obtained from a Milli-Q Water System (Millipore Corporation, Bedford, MA, USA). Ethanol and xylene were purchased from Sinopharm Chemical Reagent Co. Ltd. (Shanghai, China).

2.2. Sample preparation

The root and rhizome of *P. notoginseng* were collected from *P. notoginseng* planting base in the Yunnan province of China. Fresh *P. notoginseng* samples were stored in −80 °C refrigerator. The rhizome, main root, branch root, and fibrous root of *P. notoginseng* were all cut into 20 μm tissue sections using a cryostat microtome (Thermo CryoStar NX50 NOVPD, Bremen, Germany). Then, the tissue sections were mounted onto conductive side of indium tin oxide (ITO)-coated glass slide. Three adjacent branch root sections were prepared for the optimization of MALDI matrix. Steamed *P. notoginseng* samples were prepared by steaming the raw *P. notoginseng* root and rhizome in an autoclave for 20 min, 1 h, and 2 h at 110°C.

2.3. Matrix coating

After drying in vacuum for 20 min, the *P. notoginseng* tissue sections were coated with MALDI matrix. The matrix coating was carried out on a HTX TM-Sprayer™ (HTX Technologies, Carrboro, NC). 9-AA, CHCA, and 1,5-DAN were successively used as MALDI matrix for metabolites MS imaging. Since more metabolites can be detected, 1,5-DAN, 2.0 mg/mL in ACN/H_2O (70:30, v/v), was finally selected as the MALDI matrix. The flow rate of matrix solution was set to 0.05 mL/min at 60 °C. Nozzle nitrogen gas pressure was set to 10 psi. Track speed, track spacing, and nozzle-to-target distance were set to 800 mm/min, 3 mm, and 4 cm, respectively. A total of six spray cycles were made over each tissue sections.

2.4. MALDI-MSI experiment

MALDI-MSI experiment was performed on a RapifleX MALDI Tissuetyper™ TOF/TOF MS (Bruker Daltonics, Billerica, MA) equipped with a smartbeam™ 3D laser. The laser was fired at a repetition rate of 5000 Hz and the spatial resolution was set to 100 μm. Number of shot was set to 200. Ion source voltage 1 and Ion source voltage 2 were set to 20 kV and 17.42 kV. Lens voltage was 11.6 kV. LasAtten was set to 30%. The raw mass spectral data were acquired in both positive and negative ion modes over the range of *m/z* 80-2000. For MALDI-MS/MS experiment, the ions of interest were listed as the targets in MS/MS scan mode. The fragment shot was set to 4000. The isolation window was selected according to the system recommendation. Default isolation window is 0.6% of precursor. The MS images were viewed and processed by using FlexImaging 5.0 software (Bruker Daltonics) and SCiLS Lab 2018b software (GmbH, Bremen, Germany). To directly compare the relative contents and distributions of metabolites in different *P. notoginseng* tissue sections, we import the MALDI-MSI data of different tissue sections into one file by SCiLS Lab 2018b software.
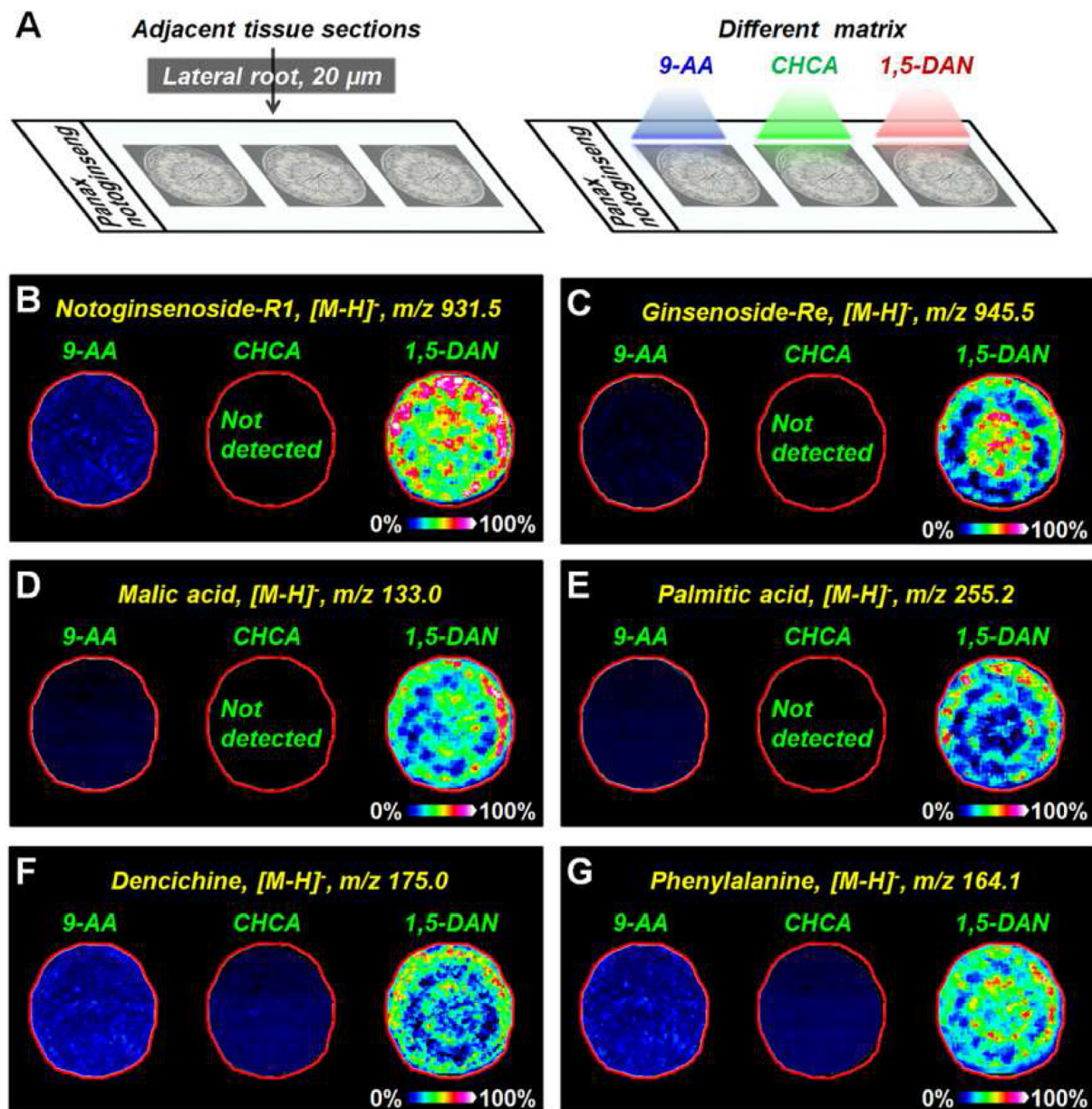
Fig. 1. (A) Optimization of matrix for MALDI-MSI of *P. notoginseng*. (B-G) Comparison of 9-AA, CHCA, and 1,5-DAN as matrices for metabolites imaging in *P. notoginseng* root section.

3. Results and discussion

3.1. Optimization of MALDI matrix for metabolite imaging in P. notoginseng

Choosing appropriate MALDI matrix is key for imaging more metabolites with high sensitivity. *P. notoginseng* contains a variety of natural products, mainly including primary metabolites such as fatty acids, amino acids and secondary metabolites such as noto-ginsenosides, ginsenosides, dencichine, etc. Amino acids and fatty acids are indispensable for cell energy metabolism and signal transduction. Dencichine, notoginsenosides, and ginsenosides are the material basis for *P. notoginseng* to treat cardiovascular and hematological diseases. Fatty acids, amino acids and dencichine contain carboxyl group, while notoginsenosides, ginsenosides contain multiple hydroxyl groups in their structure, which makes them easier to be detected in negative ion modes. 9-AA and 1,5-

DAN are two most commonly used MALDI matrices in negative ion mode. Due to their low background interference and high sensitivity, 9-AA and 1,5-DAN have been successfully used for imaging the spatial locations of phenolic acids, carbohydrates, flavones, and flavone glycosides in different plant tissues [24]. CHCA was also reported to be an effective matrix for low-molecular-weight metabolites detection [27].

In this study, to acquire more abundant metabolites information, we compared the performance of MALDI-MSI on detecting metabolites in the root of *P. notoginseng* using 9-AA, CHCA, and 1,5-DAN as matrix. As shown in Fig. 1A, three adjacent sections from the same *P. notoginseng* root were subjected to MALDI-MSI analysis after spraying CHCA, 9-AA, and 1,5-DAN, respectively. The results suggest that all the detected primary and secondary metabolites exhibited stronger ion intensities when 1,5-DAN were used as MALDI matrix. For example, notoginsenoside-R1 (Fig. 1B, [M-H]⁻, m/z 931.5), ginsenoside-Re (Fig. 1C, [M-H]⁻, m/z 945.5), malic acid
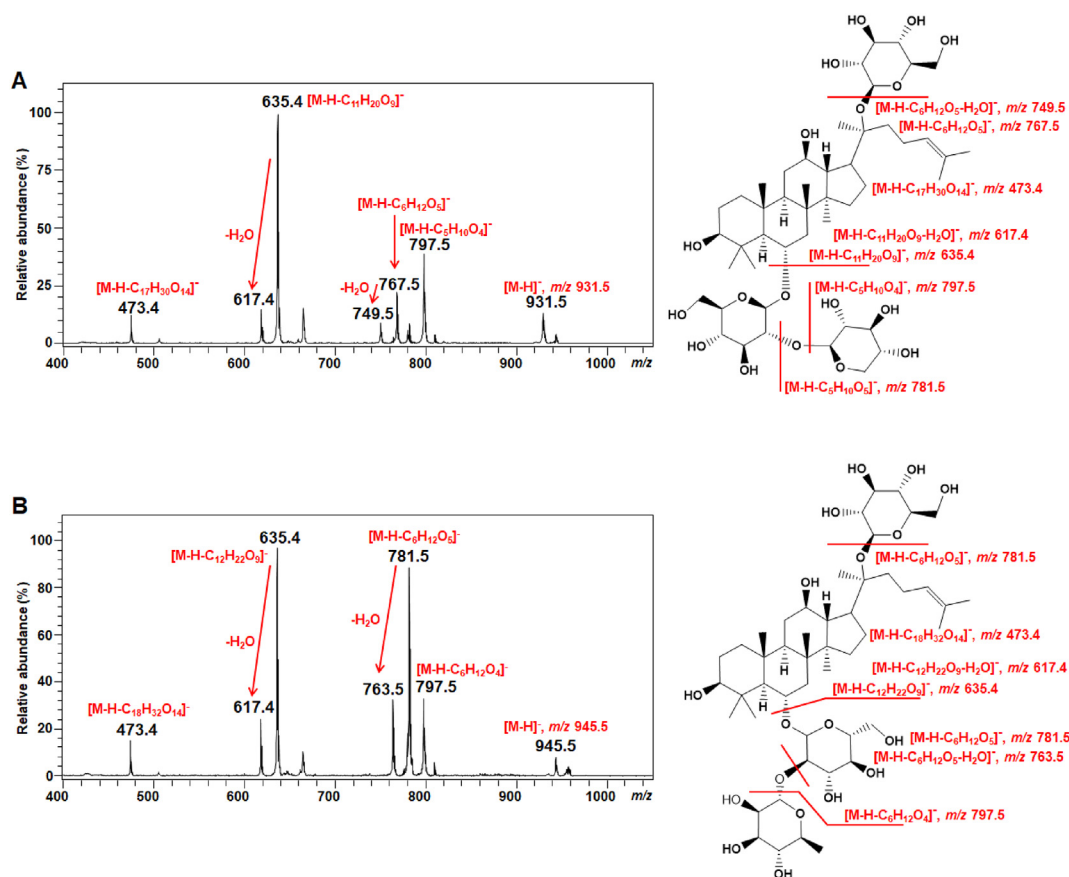
Fig. 2. *In situ* MS/MS spectra of notoginsenoside-R1 (A) and ginsenoside-Re (B).

(Fig. 1D, [M-H]⁻, *m/z* 133.0), and palmitic acid (Fig. 1E, [M-H]⁻, *m/z* 255.2) cannot be detected when CHCA was used as matrix. Although the spatial locations of notoginsenoside-R1, ginsenoside-Re, malic acid, palmitic acid, dencichine (Fig. 1F, [M-H]⁻, *m/z* 175.0) and phenylalanine (Fig. 1G, [M-H]⁻, *m/z* 164.1) all can be imaged when 9-AA and 1,5-DAN were used as matrix, stronger ion intensities could be achieved for MALDI-MSI with 1,5-DAN as compared with 9-AA.

Furthermore, we carried out *in situ* MS/MS experiment directly in the tissue regions with high metabolite levels on *P. notoginseng* root sections. Fig. 2 illustrates the typical *in situ* MALDI-MS/MS spectra and the fragmentation pathways of notoginsenoside-R1 and ginsenoside-Re. The results suggest that saponins tend to break glycoside bonds to generate characteristic product ions. For notoginsenoside-R1, the characteristic product ions include *m/z* 635.4 ([M-H-$C_{11}H_{20}O_9$]⁻), *m/z* 617.4 ([M-H-$C_{11}H_{20}O_9$-H_2O]⁻), *m/z* 797.5 ([M-H-$C_5H_{10}O_4$]⁻), *m/z* 767.5 ([M-H-$C_6H_{12}O_5$]⁻), *m/z* 749.5 ([M-H-$C_6H_{12}O_5$-H_2O]⁻), etc. (Fig. 2A). For ginsenoside-Re, the characteristic product ions include *m/z* 635.4 ([M-H-$C_{12}H_{22}O_9$]⁻), *m/z* 617.4 ([M-H-$C_{12}H_{22}O_9$-H_2O]⁻), *m/z* 781.5 ([M-H-$C_6H_{12}O_5$]⁻), *m/z* 763.5 ([M-H-$C_6H_{12}O_5$-H_2O]⁻), *m/z* 797.5 ([M-H-$C_6H_{12}O_4$]⁻), etc. (Fig. 2B).

3.2. Spatial distributions of metabolites in different tissues and different tissue micro-regions of P. notoginseng

According to the Safranin O-Fast Green (SOFG) stain image, *P. notoginseng* root section can be further divided into phloem, xylem, medulla, and cork tissues (Fig. 3A). The spatial distributions of different classes of metabolites in *P. notoginseng*, including notoginsenosides, ginsenosides, amino acids, dencichine, gluconic

acid, and low-molecular-weight organic acids were successfully imaged using the optimized MALDI-MSI method. For example, notoginsenoside-R1 showed stronger ion signal in the phloem and outer xylem (Fig. 3B). On the contrary, the level of ginsenoside-Re in the medulla and inner xylem is much higher than that in the phloem and outer xylem (Fig. 3C). Ginsenoside-20Rh1 was found to be mainly distributed in the phloem region (Fig. 3D). Amino acids such as phenylalanine, glutamine, and asparagine were mainly distributed in the medulla and phloem regions (Fig. 3E–G). Dencichine (Fig. 3H) and gluconic acid (Fig. 3I) presented the highest ion signal in the phloem, followed by the medulla, then the xylem. Low-molecular-weight organic acids, including malic acid (Fig. 3J) and citric acid (Fig. 3K) all exhibited stronger ion intensities in phloem and medulla than xylem. In addition, some unknown metabolite ions showed region-specific distributions in the root of *P. notoginseng*. For instance, the metabolite ions of *m/z* 274.2 and *m/z* 288.2 mainly distributed in the phloem region (Fig. 3L and M); the metabolite ion of *m/z* 594.3 exhibited stronger ion intensity in the xylem region (Fig. 3N); the metabolite ion of m/z 795.5 was more expressed in the cork layer region (Fig. 3O).

The rhizome and root of *P. notoginseng* have long been used for the treatment of hematological and cardiovascular diseases. Actually, the root of *P. notoginseng* includes main root, branch root and fibrous root. Fig. 4A and Fig. 4B illustrate the optical photo and SOFG stain image of *P. notoginseng* rhizome, main root, branch root and fibrous root. In this study, we carried out MALDI-MSI analysis on rhizome, main root, branch root and fibrous root from the same *P. notoginseng* plant. Furthermore, we conducted principal component analysis (PCA) based on the *in situ* MALDI-MS spectra of rhizome and different root tissue sections. A clear indication of
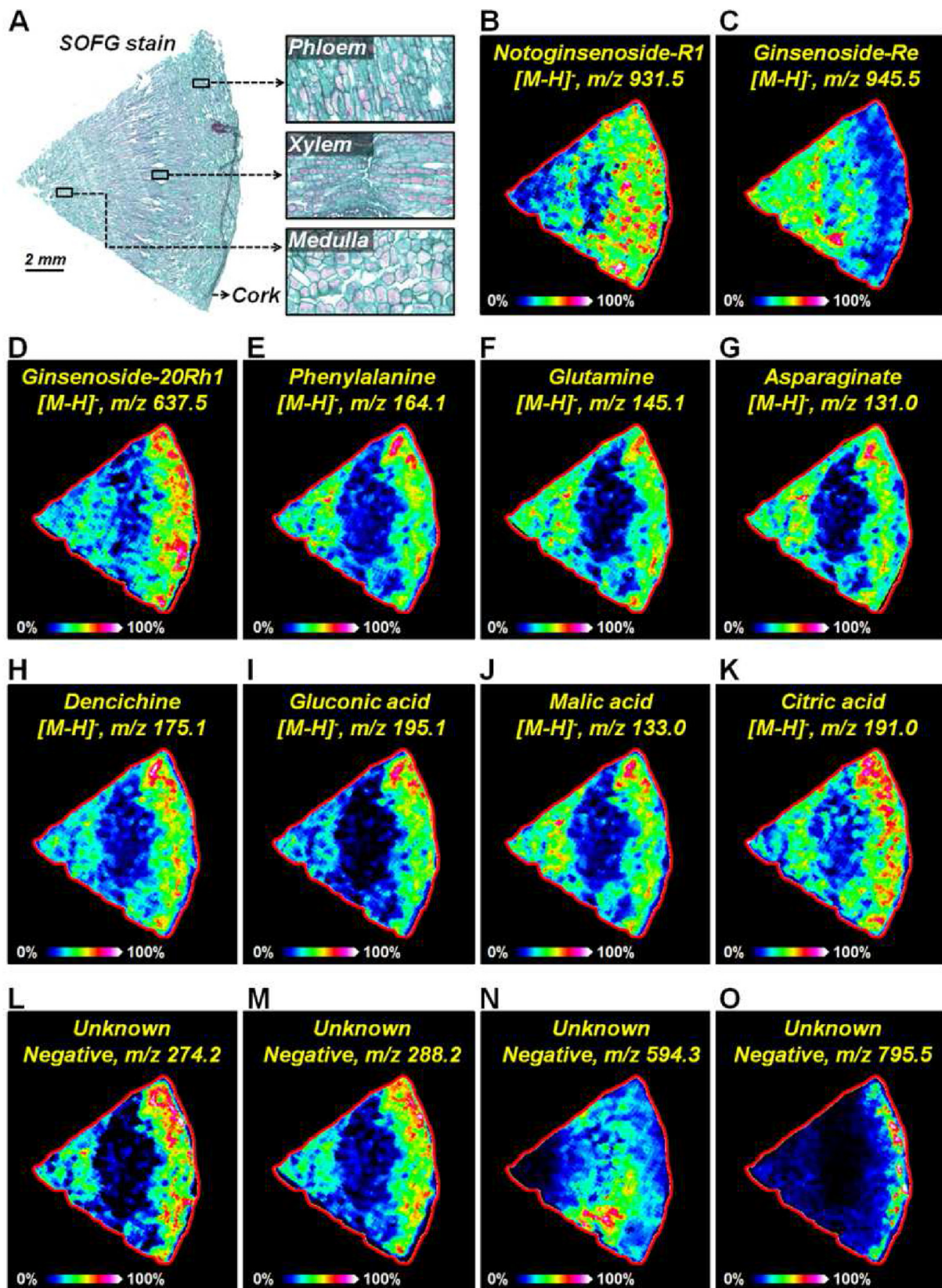
Fig. 3. MS images of representative metabolites in *P. notoginseng* root section.

separation was observed between rhizome and root tissues (Fig. 4C), which indicated that the metabolite profile of *P. notoginseng* rhizome was very different from that of *P. notoginseng* root. The MS images of representative metabolites in rhizome and different root tissue sections were shown in Fig. 4D–L. The levels of notoginsenoside-R1 in rhizome and different root tissues were similar (Fig. 4D). Other saponins, such as notoginsenoside-Fc and ginsenoside-Re, were more expressed in the rhizome tissue (Fig. 4E and F). The result was consistent with the report by Wang et al [10]. The levels of dencichine (Fig. 4G) and citric acid (Fig. 4H) in main root were much higher than that in rhizome, branch root and fibrous root. Glutamine (Fig. 4I) and asparagine (Fig. 4J) presented much stronger ion signals in rhizome than root tissues. The metabolite ion m/z 221.1 was mainly distributed in main root tissue (Fig. 4K). The metabolite ion m/z 624.5 is almost exclusively expressed in rhizome (Fig. 4L).

3.3. Spatiotemporal changes of metabolites during *P. notoginseng* steaming

Both raw and steamed *P. notoginseng* were recognized as important medicine for the treatment of various diseases. The alteration of metabolites during the steaming process is regarded as an important reason for the difference of pharmacological effects between raw and steamed *P. notoginseng*. MALDI-MS imaging offers an efficient approach to explore the spatiotemporal alterations of

metabolites during the steaming of *P. notoginseng*. In this study, we divided a *P. notoginseng* root tissue into four equal parts, one part was not steamed, and the other three parts were steamed in 110°C for 20 min, 1 h and 2 h, respectively (Fig. 5A). Then, one raw and three steamed *P. notoginseng* root tissues were cut into 20 μm tissue sections and subjected to MALDI-MS imaging analysis. The results are shown in Fig. 5B, C, and Fig. 5D. The levels of notoginsenoside-R1 (Fig. 5B1), notoginsenoside-Fc (Fig. 5B2), and ginsenoside-Re (Fig. 5B3) in raw and steamed *P. notoginseng* root differ slightly. Therefore, the high-abundance saponins such as notoginsenoside-R1, notoginsenoside-Fc, and ginsenoside-Re may not be the main reason for the biological difference between raw and steamed *P. notoginseng*. However, previous studies based on HPLC technique have found that notoginsenoside-R1 and ginsenoside-Re *P. notoginseng* were decreased gradually during the steaming process [3,28], which was different from our results. This may be due to the fact that the samples analyzed by MALDI-MSI were from the same cross-section of a certain *P. notoginseng* root, while the HPLC analysis was carried out on the mixed extracts of many *P. notoginseng* roots. Dencichine is the main hemostatic component in *P. notoginseng*. The MALDI-MSI results suggest that the content of dencichine in the roots of *P. notoginseng* decreased significantly after steaming (Fig. 5C1), which corresponds to the better hemostatic effect of raw *P. notoginseng*. Arginine and glutamine are two important amino acids in *P. notoginseng*. And the MALDI-MSI results suggest that their contents gradually increase with the
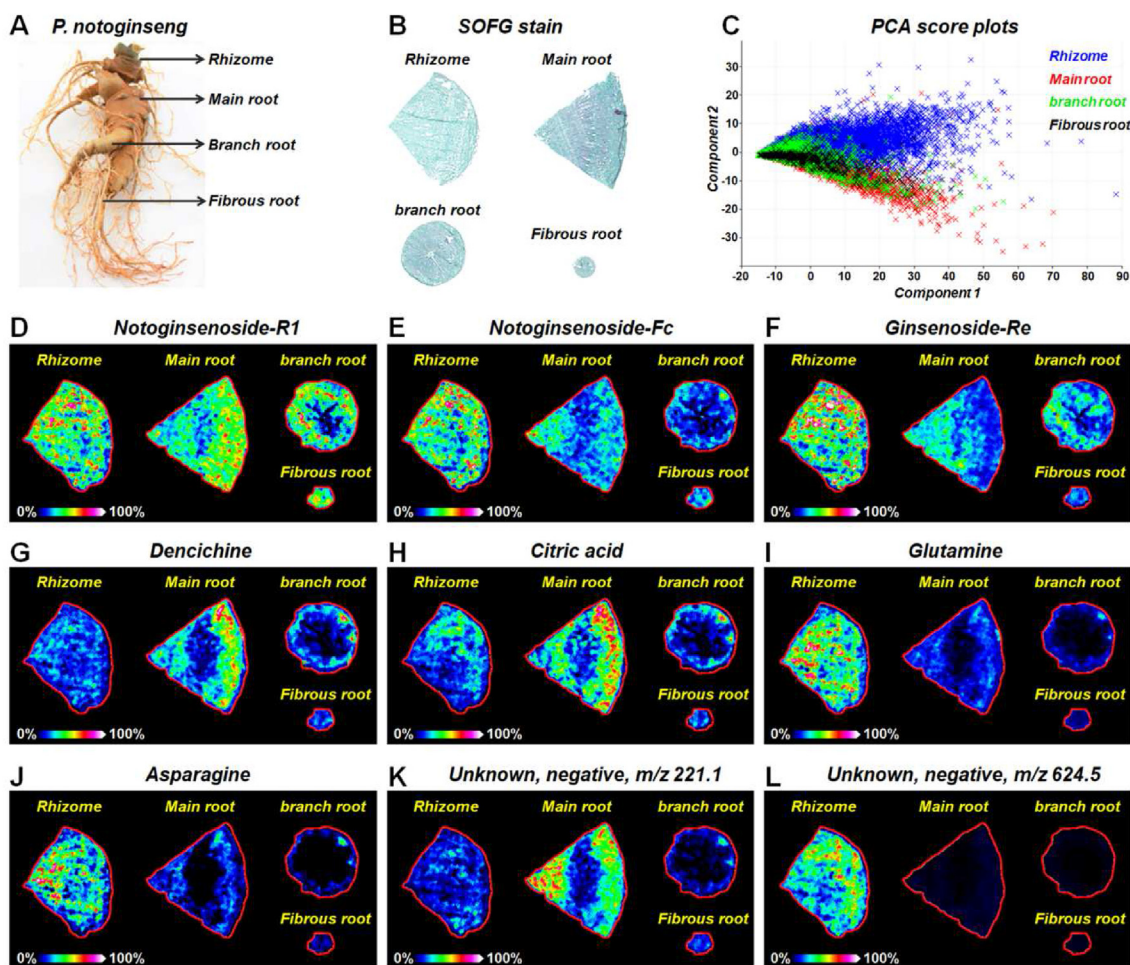

Fig. 4. (A) Optical photo of *P. notoginseng*. (B) Safranin O-Fast Green (SOFG) stain image of *P. notoginseng* rhizome, main root, branch root, and fibrous root. (C) PCA score plot based on the MALDI-MS data of different *P. notoginseng* tissue sections. (D-L) MS images of representative metabolites in *P. notoginseng* rhizome, main root, branch root, and fibrous root.
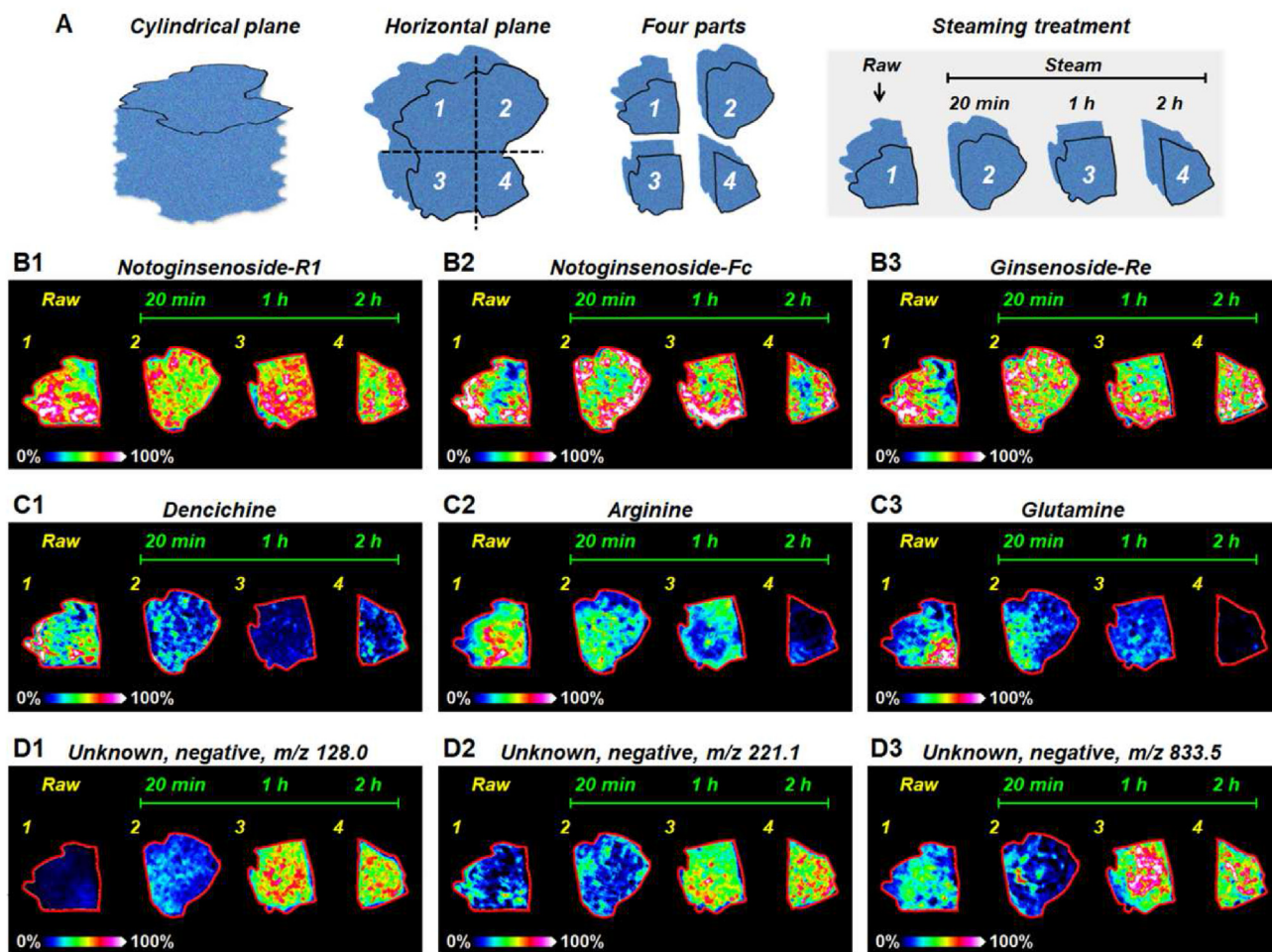
Fig. 5. (A) The process of obtaining raw and steamed *P. notoginseng* tissues from same *P. notoginseng* root. (B-D) MS images of representative metabolites in raw and steamed *P. notoginseng* root sections.

extension of steaming time (Fig. 5C2 and Fig. 5C3). Some metabolite ions such as *m/z* 128.0, *m/z* 221.1, and *m/z* 833.5 showed very low intensities in raw *P. notoginseng*. However, as the steaming progresses, their signal intensities have increased significantly (Fig. 5D). These metabolites, which changed with steaming, may be the main cause of the different pharmacological effects of raw and steamed *P. notoginseng*.

4. Conclusion

In this study, a high-coverage MALDI-MS imaging was developed to image the spatial distributions of notoginsenosides, ginsenosides, amino acids, dencichine, gluconic acid, and low-molecular-weight organic acids in *P. notoginseng* root and rhizome. The underlying metabolite information contained in different locations of *P. notoginseng* (including rhizome, main root, branch root and fibrous root) and in different micro-regions of *P. notoginseng* root (including phloem, xylem, medulla, and cork) were successfully imaged for the first time. Moreover, we investigated the spatiotemporal changes of metabolites during the steaming of *P. notoginseng* root, and screened out a series of metabolites that changed with the steaming process. Imaging the spatial locations of metabolites in different tissue regions of *P. notoginseng* not only offers a new approach to understand the complex plant metabolic pathways, but also helps to visualize the

spatiotemporal changes of metabolites during *P. notoginseng* steaming.

Declaration of competing interest

The authors declare no conflict of interest.

References

[1] Chan HH, Hwang TL, Reddy MV, Li DT, Qian K, Bastow KF, et al. Bioactive constituents from the roots of Panax japonicus var. major and development of a LC-MS/MS method for distinguishing between natural and artifactual compounds. J Nat Prod 2011;74:796–802.

[2] Liu F, Ma N, He C, Hu Y, Li P, Chen M, et al. Qualitative and quantitative analysis of the saponins in Panax notoginseng leaves using ultra-performance liquid chromatography coupled with time-of-flight tandem mass spectrometry and high performance liquid chromatography coupled with UV detector. J Ginseng Res 2018;42:149–57.

[3] Xiong Y, Chen L, Man J, Hu Y, Cui X. Chemical and bioactive comparison of Panax notoginseng root and rhizome in raw and steamed forms. J Ginseng Res 2019;43:385–93.

[4] Zhu D, Zhou Q, Li H, Li S, Dong Z, Li D, et al. Pharmacokinetic characteristics of steamed notoginseng by an efficient LC-MS/MS method for simultaneously quantifying twenty-three triterpenoids. J Agric Food Chem 2018;66:8187–98.

[5] Lu YY, Song JY, Li Y, Meng YQ, Zhao MB, Jiang Y, et al. Comparative study on excretive characterization of main components in herb pair notoginseng-safflower and single herbs by LC-MS/MS. Pharmaceutics 2018;10.

[6] Xu C, Wang W, Wang B, Zhang T, Cui X, Pu Y, et al. Analytical methods and biological activities of Panax notoginseng saponins: recent trends. J Ethnopharmacol 2019;236:443–65.

[7] Yang Z, Zhu J, Zhang H, Fan X. Investigating chemical features of Panax notoginseng based on integrating HPLC fingerprinting and determination of multiconstituents by single reference standard. J Ginseng Res 2018;42:334–42.

[8] Shimizu T, Watanabe M, Fernie AR, Tohge T. Targeted LC-MS analysis for plant secondary metabolites. Methods Mol Biol 2018;1778:171–81.

[9] Wolfender JL, Marti G, Thomas A, Bertrand S. Current approaches and challenges for the metabolite profiling of complex natural extracts. J Chromatogr A 2015;1382:136–64.

[10] Wang J-R, Yau L-F, Gao W-N, Liu Y, Yick P-W, Liu L, et al. Quantitative comparison and metabolite profiling of saponins in different parts of the root of Panax notoginseng. J Agric Food Chem 2014;62:9024–34.

[11] Boughton BA, Thinagaran D, Sarabia D, Bacic A, Roessner U. Mass spectrometry imaging for plant biology: a review. Phytochem Rev 2016;15:445–88.

[12] Feenstra AD, Alexander LE, Song Z, Korte AR, Yandeau-Nelson MD, Nikolau BJ, et al. Spatial mapping and profiling of metabolite distributions during germination. Plant Physiol 2017;174:2532–48.

[13] Norris JL, Caprioli RM. Analysis of tissue specimens by matrix-assisted laser desorption/ionization imaging mass spectrometry in biological and clinical research. Chem Rev 2013;113:2309–42.

[14] Sun C, Li Z, Ma C, Zang Q, Li J, Liu W, et al. Acetone immersion enhanced MALDI-MS imaging of small molecule metabolites in biological tissues. J Pharm Biomed Anal 2019;176:112747.

[15] Lee YJ, Perdian DC, Song Z, Yeung ES, Nikolau BJ. Use of mass spectrometry for imaging metabolites in plants. Plant J 2012;70:81–95.

[16] Dong Y, Li B, Aharoni A. More than pictures: when MS imaging meets histology. Trends Plant Sci 2016;21:686–98.

[17] Bhandari DR, Wang Q, Friedt W, Spengler B, Gottwald S, Rompp A. High resolution mass spectrometry imaging of plant tissues: towards a plant metabolite atlas. Analyst 2015;140:7696–709.

[18] Li B, Neumann EK, Ge J, Gao W, Yang H, Li P, et al. Interrogation of spatial metabolome of Ginkgo biloba with high-resolution matrix-assisted laser desorption/ionization and laser desorption/ionization mass spectrometry imaging. Plant, Cell Environ 2018;41:2693–703.

[19] Horn PJ, Korte AR, Neogi PB, Ebony L, Johannes F, Kerstin S, et al. Spatial mapping of lipids at cellular resolution in embryos of cotton. Plant Cell 2012;24:622–36.

[20] Woodfield HK, Sturtevant D, Borisjuk L, Munz E, Guschina IA, Chapman K, et al. Spatial and temporal mapping of key lipid species in Brassica napus seeds. Plant Physiol 2017;173:1998–2009.

[21] Sun C, Liu W, Ma S, Zhang M, Geng Y, Wang X. Development of a high-coverage matrix-assisted laser desorption/ionization mass spectrometry imaging method for visualizing the spatial dynamics of functional metabolites in Salvia miltiorrhiza Bge. J Chromatogr A 2020;1614:460704.

[22] Bin L, Camilla K, Natascha Krahl H, Kirsten JR, Rubini K, SRen B, et al. Visualizing metabolite distribution and enzymatic conversion in plant tissues by desorption electrospray ionization mass spectrometry imaging. Plant J 2013;74:1059–71.

[23] Tocci N, Gaid M, Kaftan F, Belkheir AK, Belhadj I, Liu B, et al. Exodermis and endodermis are the sites of xanthone biosynthesis in Hypericum perforatum roots. New Phytol 2018;217:1099–112.

[24] Sun C, Zhang M, Dong H, Liu W, Guo L, Wang X. A spatially-resolved approach to visualize the distribution and biosynthesis of flavones in Scutellaria baicalensis Georgi. J Pharm Biomed Anal 2020;179:113014.

[25] Shroff R, Vergara F, Muck A, Svatos A, Gershenzon J. Nonuniform distribution of glucosinolates in Arabidopsis thaliana leaves has important consequences for plant defense. Proc Natl Acad Sci U S A 2008;105:6196–201.

[26] Manuela P, Johannes T, Darin P, Winfriede W, Wim VDE, Hans-Peter M, et al. Spatio-temporal dynamics of fructan metabolism in developing barley grains. Plant Cell 2014;26:3728.

[27] Porta T, Grivet C, Knochenmuss R, Varesio E, Hopfgartner G. Alternative CHCA-based matrices for the analysis of low molecular weight compounds by UV-MALDI-tandem mass spectrometry. J Mass Spectrom 2011;46:144–52.

[28] Wang D, Liao P-Y, Zhu H-T, Chen K-K, Xu M, Zhang Y-J, et al. The processing of Panax notoginseng and the transformation of its saponin components. Food Chem 2012;132:1808–13.